International Journal of Oil, Gas and Coal Engineering
2023; 11(2): 47-52
http://www.sciencepublishinggroup.com/j/ogce
doi: 10.11648/j.ogce.20231102.13
ISSN: 2376-7669 (Print); ISSN: 2376-7677 (Online)

A S-wave Spectral Decomposition Hydrocarbon Detection Method Based on P-wave and S-wave Source and Its Application

Qian Zhao, Zhigang Chen, Hui Ma, Xing Sun, Yan Wang, Jianming Guo, Jiru Guo

Geological Research Center, Bureau of Geophysical Prospect, Zhuozhou, China

Email address:
530878453@qq.com (Qian Zhao)

To cite this article:
Qian Zhao, Zhigang Chen, Hui Ma, Xing Sun, Yan Wang, Jianming Guo, Jiru Guo. A S-wave Spectral Decomposition Hydrocarbon Detection Method Based on P-wave and S-wave Source and Its Application. *International Journal of Oil, Gas and Coal Engineering*. Vol. 11, No. 2, 2023, pp. 47-52. doi: 10.11648/j.ogce.20231102.13

Received: March 26, 2023; **Accepted**: April 26, 2023; **Published**: May 10, 2023

Abstract: S-wave source vector exploration is a promising technology in future seismic exploration. Conventional P-wave and S-wave joint inversion methods for hydrocarbon detection are limited in some aspects. First, P-wave and S-wave joint inversion is mainly based on the converted wave theory, but no theoretical support for S-wave generated by S-wave source. Second, the inversion method is complex and difficult to operate. Because P-wave and S-wave from S-wave source should accurately match with each other, without an effective approach, it has to follow the method of P-wave matching with converted wave, so it is not helpful to extensive application. This paper proposes a comprehensive s-wave spectral decomposition hydrocarbon detection method based on p-wave and s-wave source. First, the velocity ratio of P-wave to S-wave (Vp/Vs ratio) is derived to be equal to the frequency notch period ratio of P-wave to S-wave, and approximately equal to the dominant frequency ratio of P-wave to S-wave. Second, spectral decomposition is conducted at the target layer to obtain the tuning frequency spectra of P-wave and S-wave seismic data, respectively, and the dominant frequencies of P-wave and S-wave are automatically identified. Third, the Vp/Vs ratio and Poisson's ratio are calculated according to the dominant frequency ratio of P-wave to S-wave for final hydrocarbon detection. This method is independent on well data and accurate matching of P-wave with S-wave data, it is simple, quick and efficient. It's widely applicable in any areas more or less explored. Application in an oilfield in western China has obtained effective results.

Keywords: S-wave Source, Vector Exploration, P-wave and S-wave Joint Inversion, Spectral Decomposition, Hydrocarbon Detection

1. Introduction

The multi-wave and multi-component seismic exploration technology has been applied for more than 40 years since the 1970s [1-3]. Multi-wave and multi component kinematics (travel time, velocity, structure, similarity, etc.), dynamics (amplitude, frequency, phase, absorption, attenuation, dispersion, azimuth anisotropy, etc.), and the time difference ratio, amplitude ratio and velocity ratio of P-wave to S-wave are useful for comprehensive characterization of reservoir physical properties such as reservoir distribution, reservoir parameter distribution, fracture development, gas content and fluid properties [4, 13-15]. Technologies for multi-wave and multi-component seismic data acquisition and processing are more to select, but only a few for interpretation, which can be classified into three classes [5]. 1. P-wave and S-wave joint calibration technology. The geological properties of P-wave reflector and S-wave convertor are defined, and their relationship is built, based on which the characteristics and comparing principles of P-wave and S-wave groups at the stratigraphic interface are analyzed. 2. P-wave and S-wave matching technology. After calibration of P-wave and converted wave, the time of P-wave and that of converted wave are compressed or stretched, the amplitude and time are calibrated, and the frequency and phase are corrected. 3. P-wave and S-wave joint inversion technology. Using the technology, parameters such as P-wave acoustic impedance, S-wave impedance, elastic impedance, P-wave to S-wave

velocity ratio, Poisson's ratio and density are estimated for characterizing reservoir distribution and fluid properties. The EV56S S-wave vibrator developed by BGP, CNPC, which increases S-wave output power from 10,000 pounds in the 1980s to 30,000 pounds, has successfully promote multi-wave and multi-component seismic exploration to vector exploration. Conventional P-wave and S-wave joint inversion methods for hydrocarbon detection are limited in some aspects. First, P-wave and S-wave joint inversion is mainly based on the converted wave theory, but no theoretical support for S-wave generated by S-wave source [8, 9, 12]. Second, the inversion method is complex and difficult to operate. Because P-wave and the S-wave from S-wave source should accurately match with each other, without an effective approach, it has to follow the method of P-wave matching with converted wave, so it is not helpful to extensive application. This paper proposes a comprehensive spectral decomposition for hydrocarbon detection based on P-wave and the S-wave from S-wave source. Since it is independent on well data and accurate matching of P-wave with S-wave data, the method proposed is simple, quick and efficient. It's widely applicable in any areas more or less explored.

2. Method and Theory

2.1. Principle of Spectral Decomposition

Under the conditions of thin beds (non-coefficient pulse) and a long time window, the reflectivity could be treated as white noise, the amplitude spectrum is constant, and the amplitude spectrum of the Ricker wavelet is trapezoidal. After convoluting and adding noise, the amplitude spectrum of the seismic trace is trapezoidal (Figure 1a). In comparison, under the conditions of thin beds (non-coefficient pulse) and a short time window, the reflectivity shows the characteristics of periodic frequency notch spectra, and the amplitude spectrum of the Riker wavelet is trapezoidal. After convoluting and adding noise, the amplitude spectrum of the seismic traces also presents the characteristics of periodic frequency notch spectra (Figure 1b) [6, 7, 10, 11].

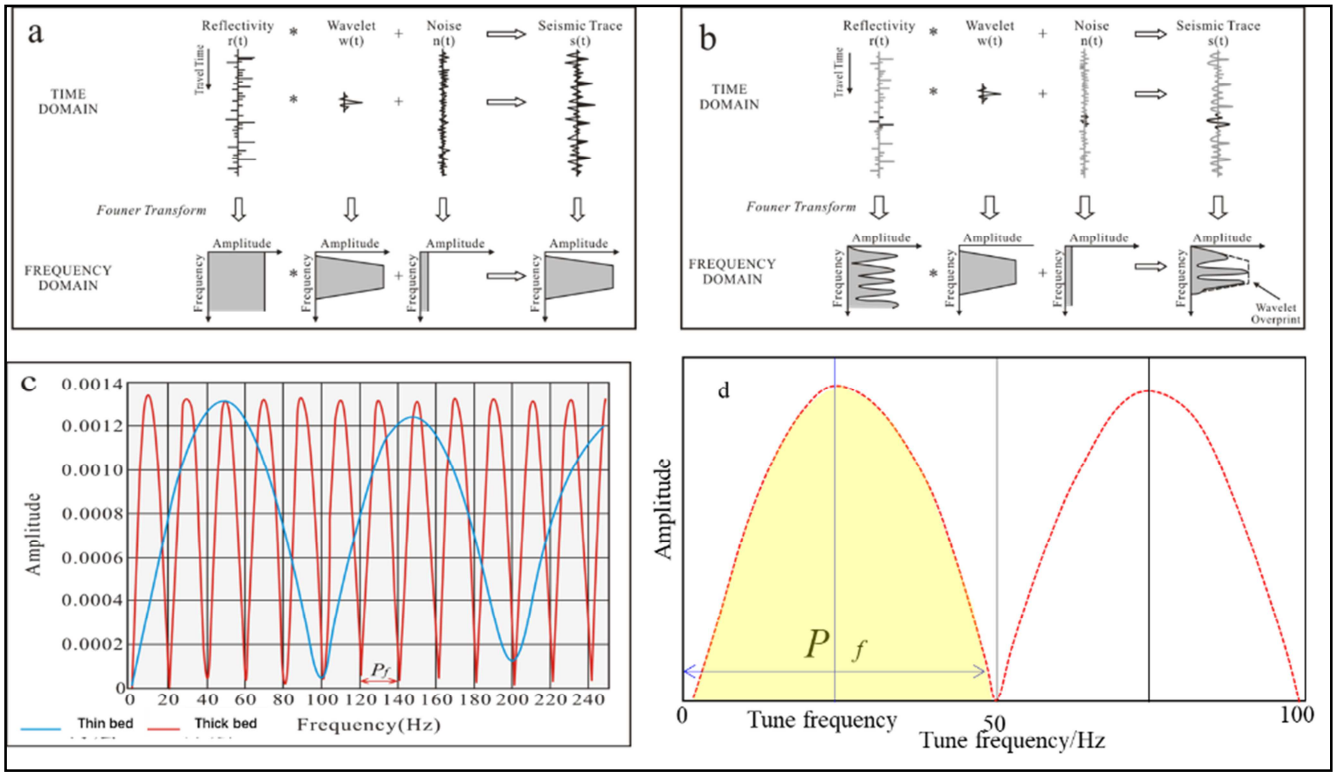

Figure 1. *Schematic diagram of spectral decomposition.*

2.2. Methods

Based on the principle of spectral decomposition, the relationship between frequency notch period and time thickness is

$$P_f = 1/\tau \tag{1}$$

Where P_f is the frequency notch period and τ is time thickness (Figure 1c). Due to

$$\tau = 2d/v \tag{2}$$

Where d is interval thickness, and v is interval velocity, so

$$P_f = v/2d \tag{3}$$

For P-wave,

$$P_p = v_p / 2d \tag{4}$$

Where P_p is frequency notch period, and v_p is p-wave velocity.

For shear wave,

$$P_s = v_s / 2d \tag{5}$$

where P_s is frequency notch period and v_s is S-wave velocity, so the velocity ratio of P-wave to S-wave is

$$v_s / v_s = P_p / P_s = \gamma \tag{6}$$

The Poisson's ratio is

$$\sigma = (\gamma^2 - 2) / 2(\gamma^2 - 1) = (P_p{}^2 - 2P_s{}^2) / 2(P_p{}^2 - P_s{}^2) \tag{7}$$

In practical applications, limited by resolution, when calculating the tuning frequency by spectral decomposition, only the first period of the frequency notch is visible, but in fact, the frequency notch period is approximately equal to twice the tuning frequency (Figure 1d), namely,

$$P_p \approx 2 f_p \tag{8}$$

$$P_S \approx 2 f_S \tag{9}$$

Take Equations (8) and (9) into Equations (6) and (7), and we will get

$$v_p / v_s = P_p / P_s \approx 2 f_p / 2 f_s = f_p / f_s \tag{10}$$

$$\sigma = (P_p{}^2 - 2P_s{}^2) / 2(P_p{}^2 - P_s{}^2) \approx (f_p{}^2 - 2 f_s{}^2) / 2(f_p{}^2 - f_s{}^2) \tag{11}$$

Therefore, the tuning frequency can be automatically picked up by spectral decomposition of the tuning spectra, and Poisson's ratio and V_P/V_S ratio can be calculated by Equations (9) and (10).

3. Examples

The study area is located between TN gas field and SB 1 gas field in the Qaidam Basin in western China. Structurally, it is located at the west wing and slope of SB 1 gas field. In the study area, the reservoirs are multi-layer loose sandstone edge-water gas reservoirs, of which the Quaternary Qigequan Formation is the pay zone. The Quaternary Qigequan Formation is distributed thick and wide, and contains many sand bodies. Affected by gas in the reservoirs, the imaging quality based on P-wave seismic data is poor. Previous reservoir prediction was only based on well data, resulting in poor prediction accuracy. In the past two years, vector exploration was carried out by shooting P-wave and S-wave with vibrators and receiving data with three-component geophones. It's the first case that nine-component seismic data were recorded in the world. After brute processing, three data sets including P-wave data, fast S-wave data and slow S-wave data have been obtained, which are basic data for seismic interpretation. The P-wave and fast and slow S-wave seismic sections are very different (Figure 2). On the P-wave seismic section, the low-frequency part of the events in the gas cloud zone at the structural high was obviously pulled down, which cannot really reflect the structural morphology. In comparison, the S-wave section reflects the structural morphology well.

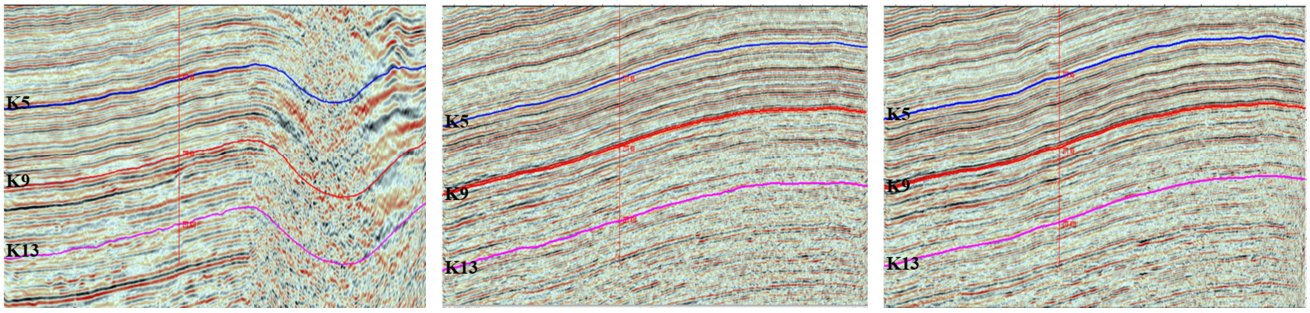

a. P-wave seismic section b. Fast S-wave seismic section c. Slow S-wave seismicsection

Figure 2. *P-wave and fast and slow S-wave seismic sections of the study area.*

3.1. Optimization of S-wave Data

When propagating in an anisotropic medium in the same direction, S-waves may split into fast and slow S-waves. As a result, two sets of seismic data, i.e., fast and slow S-waves, are obtained after brute processing. The structural maps interpreted by both fast and slow S-waves show the anticline structure in the study area (Figure 3), but there are obvious differences in structural details (Figure 3a and Figure 3b). On the TWT map of fast S-wave in K4 layer (Figure a), Wells S4-11 and S4-47 are located at the structural high, and the former is slightly higher than the latter; and the other three wells are S4-10, SX 4-14, and S27 for high to low. On the TWT map of slow S-wave in K4 layer (Figure 3b), the elevations of the 5 wells are different from theirs in Fig. 3a. S4-47 is the highest, followed by SX4-14, S4-11, S27 and S4-10 in order. Fig. 3c shows the elevations of the actual target layers of the 5 wells (red line), which are S4-11, S4-47, S4-10, SX4-14, and S27 from high to low. The elevations of the actual target layers (Figure 3c) are consistent with the elevations of the wells shown on the fast S-wave structural map (Figure 3a), indicating the fast S-wave data can more accurately reflect the real structural morphology. The RMS amplitude of fast S-wave (Figure 3d) and that of slow S-wave

(Figure 3e) picked up at the target layer (K10) are also different. Drilling data revealed that the sediment system in the study area is mainly shallow water delta with developed underwater distributary channels. The RMS amplitude of slow S-wave in K10 (Figure 3e) reflects multiple channels developed in the middle and northeast of the study area, and they are clearer than those in the RMS amplitude of fast S-wave in K10 (Figure 3d). In conclusion, fast S-wave data can better reflect the structural morphology, slow S-wave data can better reflect the reservoir, and the difference between fast S-wave and slow S-wave can reflect the anisotropy of reservoir from the principle of fast and slow S-waves generation. So the fast and slow S-waves that can better reflect reservoirs are selected for method study.

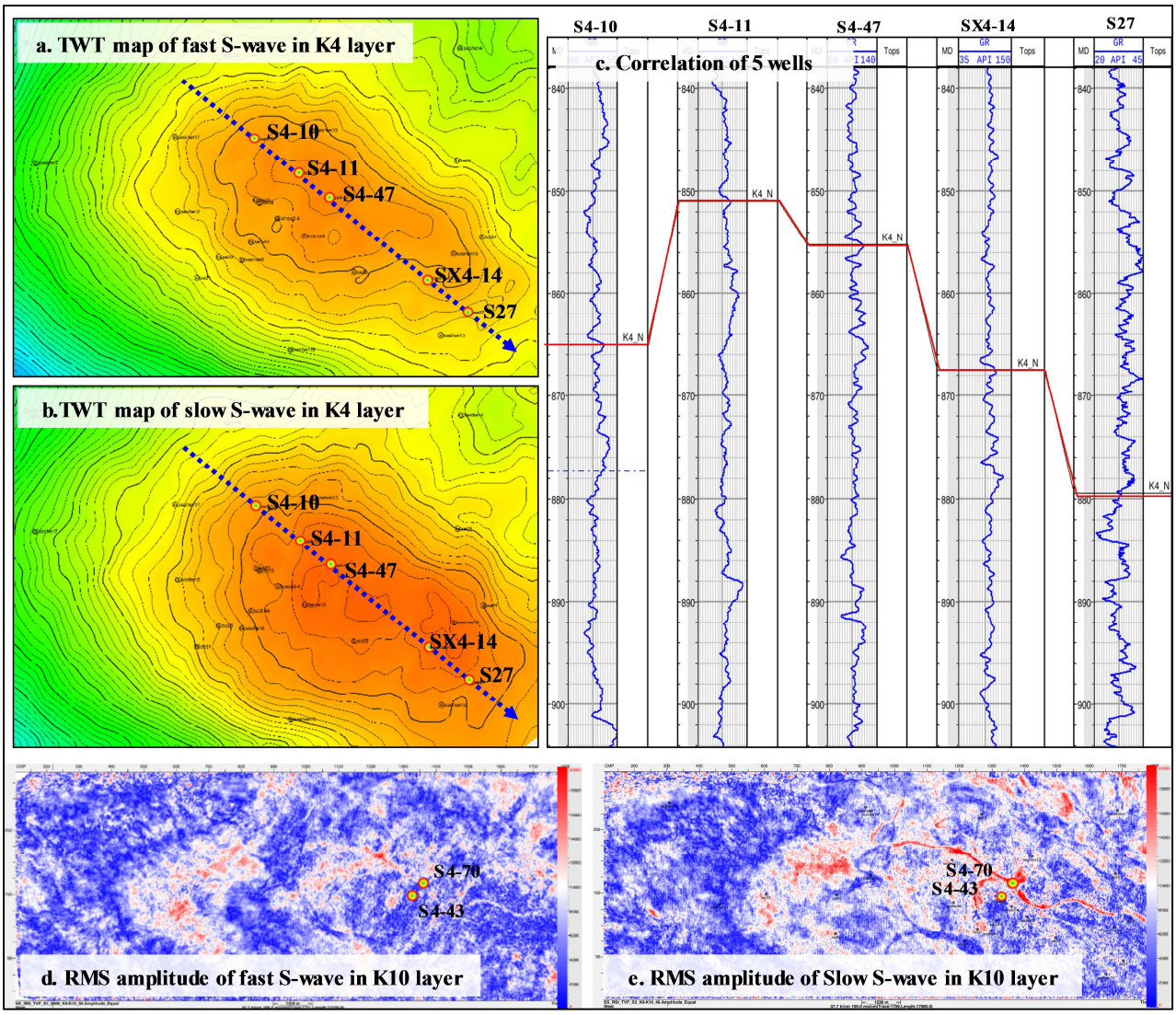

Figure 3. *Comparison of fast and slow S-wave sections.*

3.2. Spectral Decomposition of P-wave and Slow S-wave

In the study area, the dominant frequency of the P-wave data is 33 Hz, the bandwidth is 5-63 Hz, and the resolvable thickness is 15-20 m; the dominant frequency of the slow S-wave data is 32 Hz, the bandwidth is 6-59 Hz, and the resolvable sandstone layer is 6-12 m. Drilling data revealed that the thickness of the target layer was thin, and less than 8 m. After resampling the slow S-wave data at 1ms, the time window with less than 30 sampling points was used for spectral decomposition to calculate the tuning frequency of the K9 layer (one of the target layers in the study area). The maximum entropy method was used for spectral calculation. Figure 4 shows the tuning frequency spectra of the K9 layer based on P-wave and slow S-wave. The spectra of P-wave and S-wave are both convergent, indicating that the results of the tuning frequency are good. The dominant frequency was automatically picked up from the two tuning frequency spectra, which is blue in Figure 4a and pink in Figure 4b, respectively. The dominant-frequency horizon well matches the dominant frequency of the tuning spectra. Repeat the steps above to obtain the dominant frequency of P-wave and slow S-wave for other target layers.

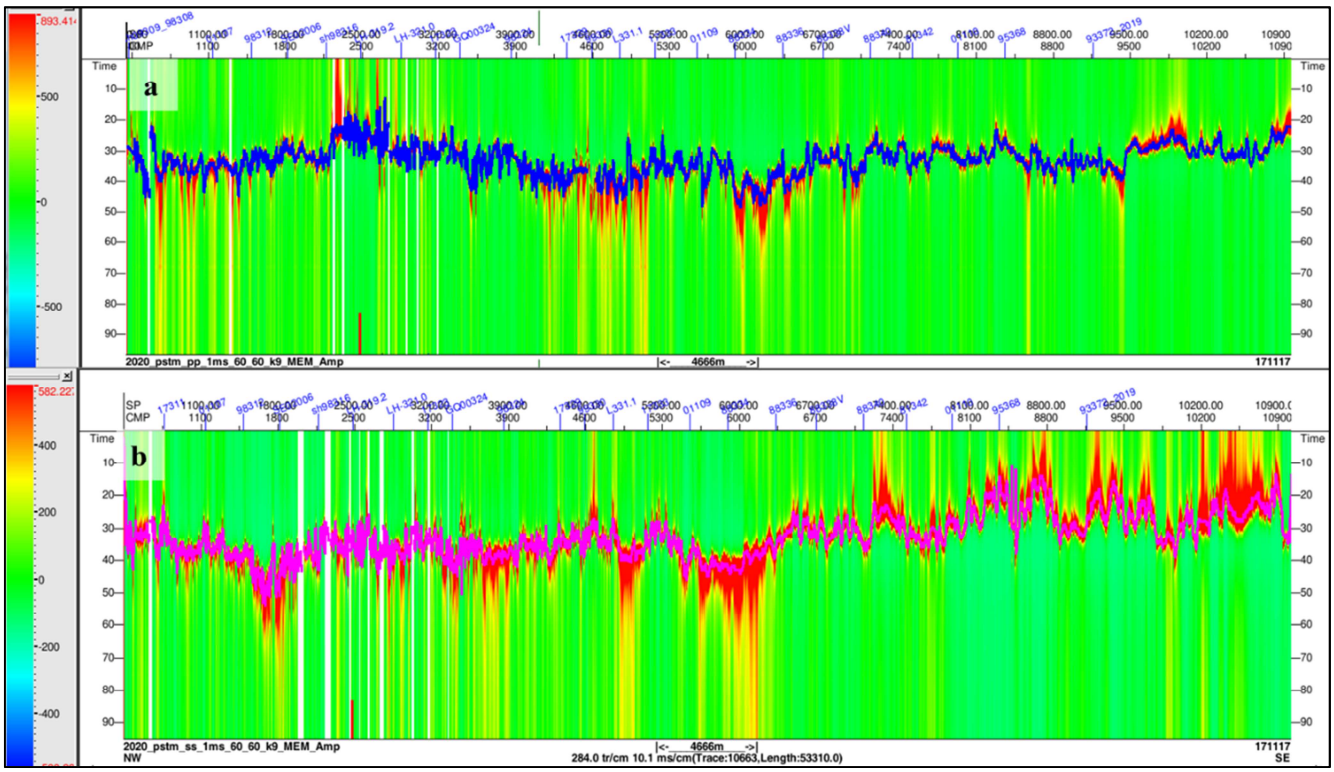

a. Tune frequency based on P-wave; b. Tune frequency based on slow S-wave

Figure 4. *Tuning frequency based on P-wave (a) and slow S-wave (b).*

3.3. Calculation of Vp/Vs Ratio

The dominant frequency in the target layer, automatically picked up through spectral decomposition, was taken into Equation (10), and the velocity ratio of P-wave to S-wave was calculated. Figure 5a, Figure 5b and Figure 5c show the velocity ratios in K4, K9 and K10, respectively. Figure 5d shows the structure map of bottom K9. The velocity ratio in every layer is almost the same as the trend of the structural morphology, namely, the structural high is a favorable gas-bearing zone, and gradually decreasing from high to low. The green in Figure 5a, 5b and 5c is caused by pull-down distortion of P-wave in the gas cloud zone at the structural high. The target layer reflected on Figure 5b and Figure 5c shows the hydrocarbon prediction trend is very coincident with the change of the structural morphology. This demonstrates the feasibility of this method proposed in this paper for hydrocarbon prediction.

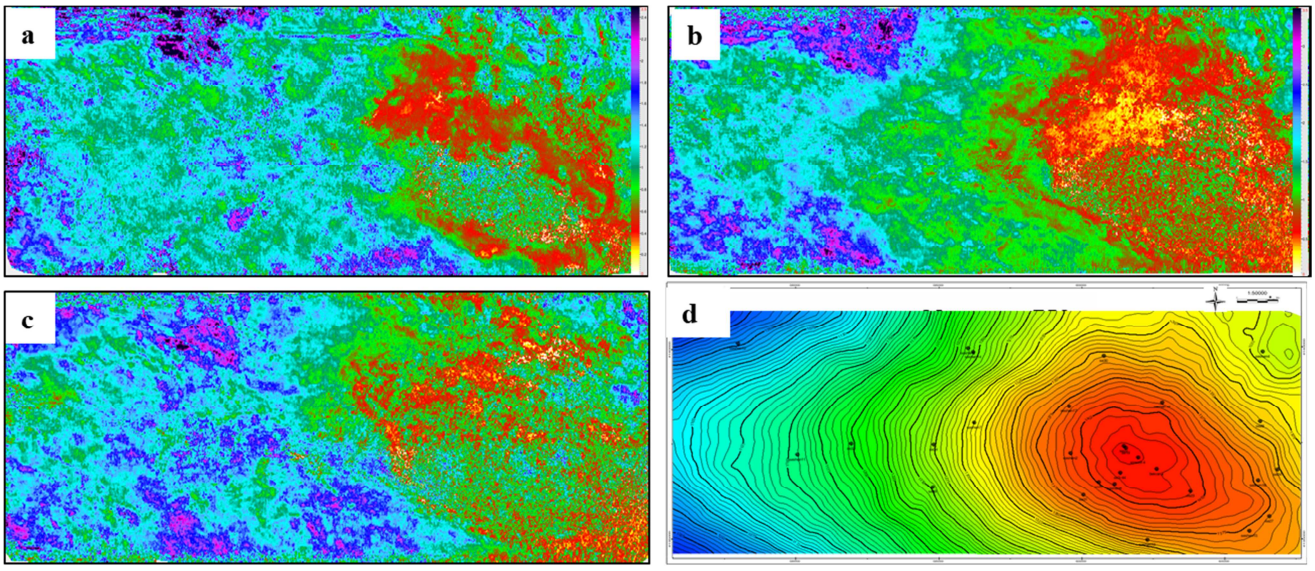

a. Vp/Vs in K4 b. Vp/Vs in K9 c. Vp/Vs in K10 d. Structure map of bottom K9

Figure 5. *Vp/Vs ratios in K4, K9 and K10 and structural map of bottom K9.*

4. Conclusion

Using P-wave and fast and slow S-waves from S-wave source, and calculating equations, first the tuning frequency in the target layer was calculated, then the dominant frequency was automatically picked up, and finally the Vp/Vs ratio and Poisson's ratio was calculated. The method is simple, quick and efficient, without matching of P-wave with S-wave and drilling data.

Fast S-wave can better reflect structural morphology, slow S-waves can better reflect reservoir, and the difference between fast and slow S-waves can reflect reservoir anisotropy.

The method has been applied in the study area and obtained good result. The hydrocarbon detection trend is well coincident with the structural morphology.

References

[1] Cafarelli B, Madtson E, Krail P. (2000) 3-D gas cloud imaging of the Donald Field with converted waves. *SEG Expanded Abstracts*. 19: 1162-1165.

[2] Hanson R, MacLeod M, Bell C, et al. (2000) 4-C seismic data and reservoir modeling at Alba Field, North Sea. *SEG Expanded Abstracts*. 19: 1453-1 455.

[3] Yao Y. (2005) Development history and prospect of multi-wave seismic exploration prospect of multi-wave seismic exploration. *Progress in Exploration Geophysics*. 28 (3), 169-173.

[4] Zhongyu H, Jianku S, Shijun Z, et al. (2007) Multi-wave and multi-component seismic technology. *Beijing: Petroleum Industry Press*. 1-114.

[5] Zhaojun M, Jianming T, Tianji X. (2010) Research progress in multi-wave and multi-component seismic exploration. *Progress in Exploration Geophysics*. 8 (33), 247-253.

[6] Xude H. (2002) Discussion on notches-in-thin-bed. *Progress in Exploration Geophysics*. 25 (5), 1-6.

[7] Morgan N. (2001) Frequencies. *Frontier.* 12, 7-9.

[8] Zhigang D. (2016) Application of multi-wave seismic exploration technology in petroleum exploration. *China Petrochem*. 24, 18-19.

[9] Ying J, et al. (2022) Joint interpretation and application of P-wave and pure S-wave. *Geophysical Prospecting for Petroleum*. 61 (06), 1053-1064.

[10] Partyka G, Gridley J, Lopdz J. (1999) Interpretational applications of spectral decomposition in reservoir characterization. *The Leading Edge*. 18 (3), 353-360.

[11] Koefored O, de Voogd N. (1980) The Linear properties of thin layers with an application to synthetic seismograns over coal seams. *Geophysics*. 45 (8), 1254-1268.

[12] Guowen C, et al. (2019) Application of PP-wave and SS-wave joint interpretation technology in gas cloud area. *Lithologic Reservoirs.* 31 (6), 79-87.

[13] Chenghong Z. (2004) Progress in multi-component seismic technology reflected from EAGE 66th annual meeting. *Progress in Exploration Geophysics.* 27 (4): 300-307.

[14] Zhongyu H, Hailong Z. (2003) Advances in converted-wave prestack migration. *Progress in Exploration Geophysics.* 26 (3), 167-171+185.

[15] Liyan Z, Yang L. (2005) Overview of prestack time migration for converted wave. *Progress in Geophysics.* 20 (4), 1134-1139.